Cell Reports, Volume *17*

Supplemental Information

Linking Memories across Time via Neuronal and Dendritic Overlaps in Model Neurons with Active Dendrites

George Kastellakis, Alcino J. Silva, and Panayiota Poirazi

Supplemental Information

Supplemental Figures

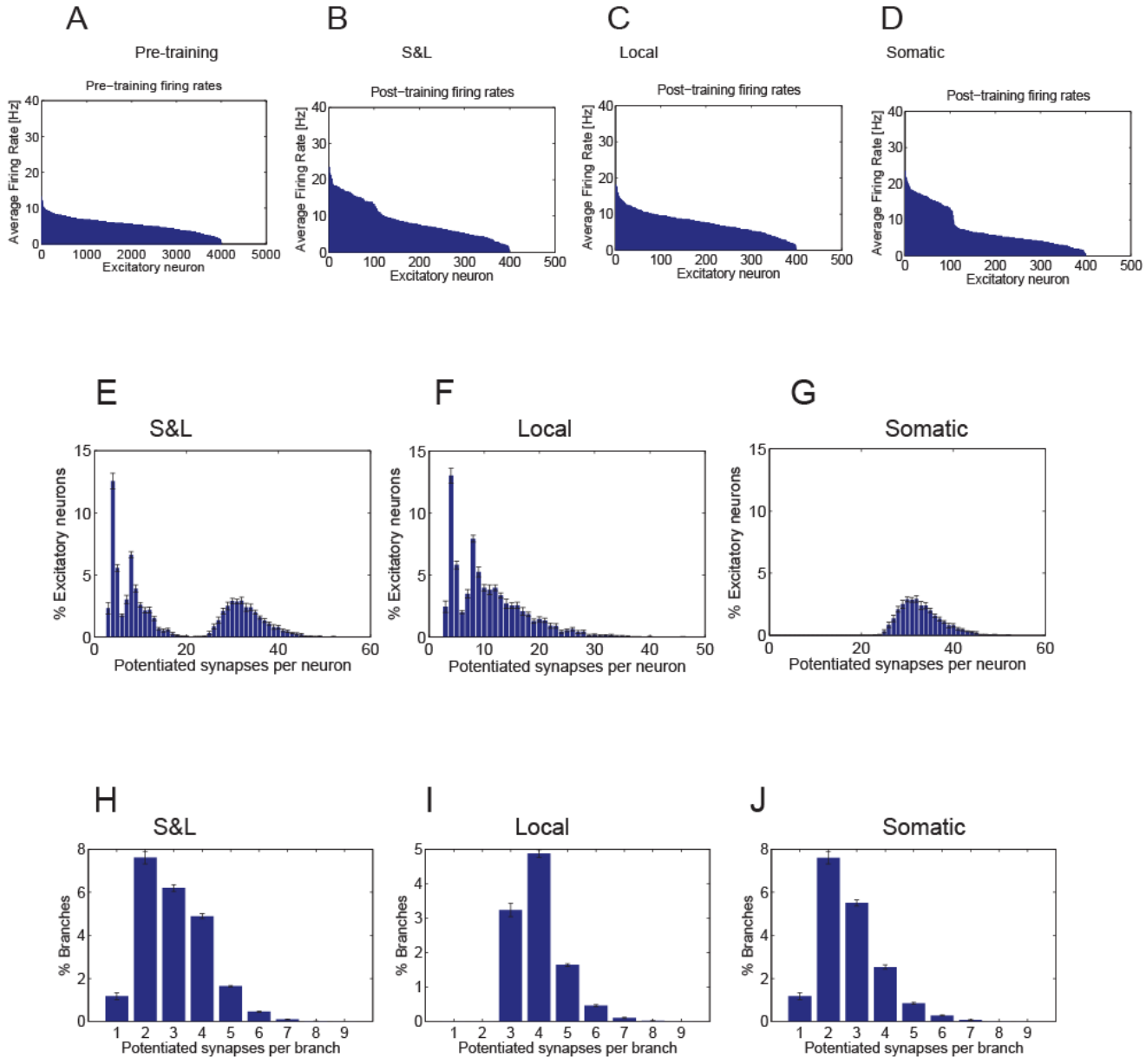

Figure S1; Related to Figure 3.

Encoding features of a single memory.

A-D) Sorted average firing rates of all excitatory neurons during recall (upon S1 presentation), before learning and after learning under the three PRP conditions.

E-G) Distribution of the number of potentiated synapses per neuron, under the three PRP conditions. Exploratory analysis (whereby increasing numbers of points from each of the three distributions are randomly drown and the resulting groups are tested as to whether they belong to the same distributions or to distinct distributions E, G or F) shows statistical significance of the difference between each pair of E, F and G required 50 neuron samples for Kruskal-Wallis test, except for the pair E & G, which required 200 neuron samples (alpha: $p<0.01$, power: $1-\beta=0.9$).

H-J) Distribution of the number of potentiated synapses per dendritic branch under the three PRP conditions. Branches without any potentiated synapses are not included. Exploratory analysis shows that statistical significance of the difference between each pair of E,F and G required 50 branch samples for Kruskal-Wallis test ($p<0.001$), except for the pair H & J, which required 20000 branch samples (alpha: $p<0.01$, power: $1-\beta=0.9$).

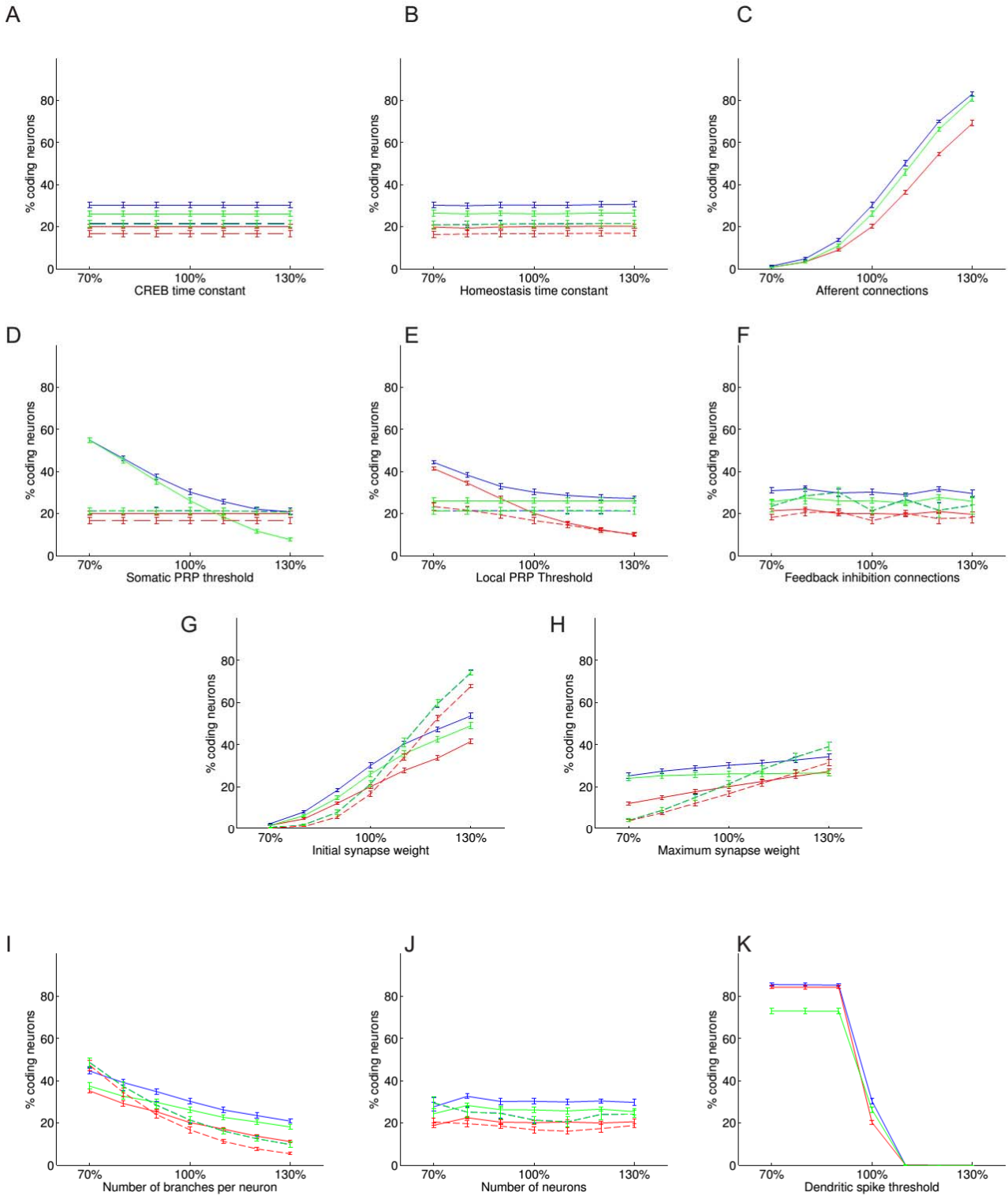

Figure S2 ; Related to Figure 2A.

Dependence of coding population size on model parameters.

A-K) Size of the neuronal population encoding a single memory under the three PRP conditions, with enhanced neuronal excitability. In each panel, a single model parameter is varied by ±30% of its original value listed in Supplemental Tables S1 & S2. Solid Blue: S&L PRPs, Solid Green: Somatic PRPs, Solid Red: local PRPs. Dashed lines indicate the PRP conditions under an alternative configuration of the model without dendritic spikes, and increased afferent connectivity to 236%. In panels C and K the alternative configuration is not shown, as these parameters were kept constant. Error bars indicate mean ± SEM of 10 trials.

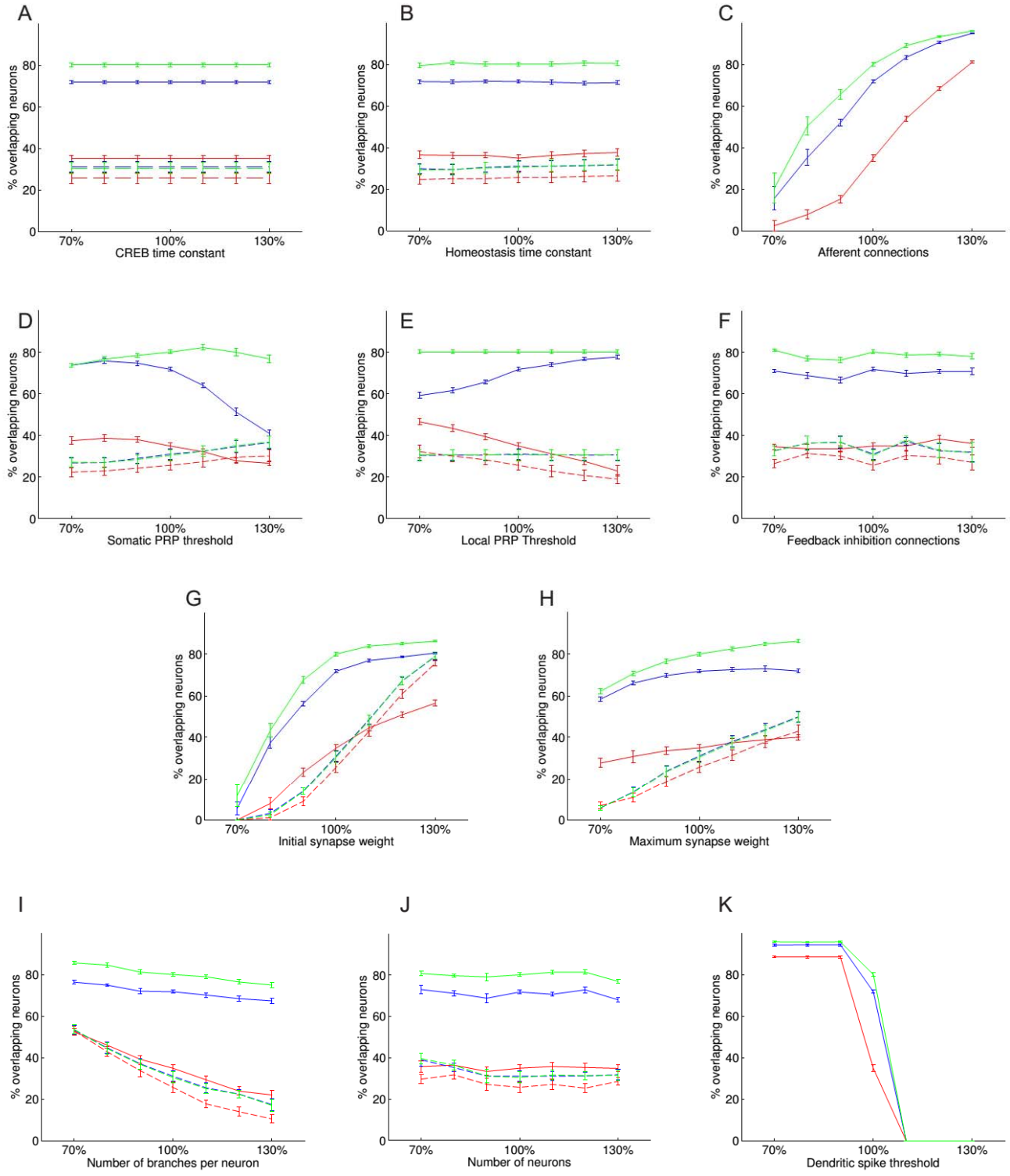

Figure S3; Related to Figure 4B.

Dependence of population overlap between weak and strong memories on model parameters.

A-K) Percentage of overlap between populations coding for weak and strong memories when the strong memory precedes the weak one by 1 hour. In each panel, a single model parameter is varied by ±30% of its original value listed in Supplemental Tables S1 & S2. Graphs show the overlap between the populations coding for the weak and strong memories after the encoding of a strong memory followed by a weak memory, under enhanced excitability conditions. Solid Blue: S&L PRPs, Solid Green: Somatic PRPs, Solid Red: local PRPs. Dashed lines indicate the PRP conditions under an alternative configuration of the model without dendritic spikes, and increased afferent connectivity to 236%. In panels C and K the alternative configuration is not shown, as these parameters were kept constant to their new values. Error bars indicate mean ± SEM of 10 trials.

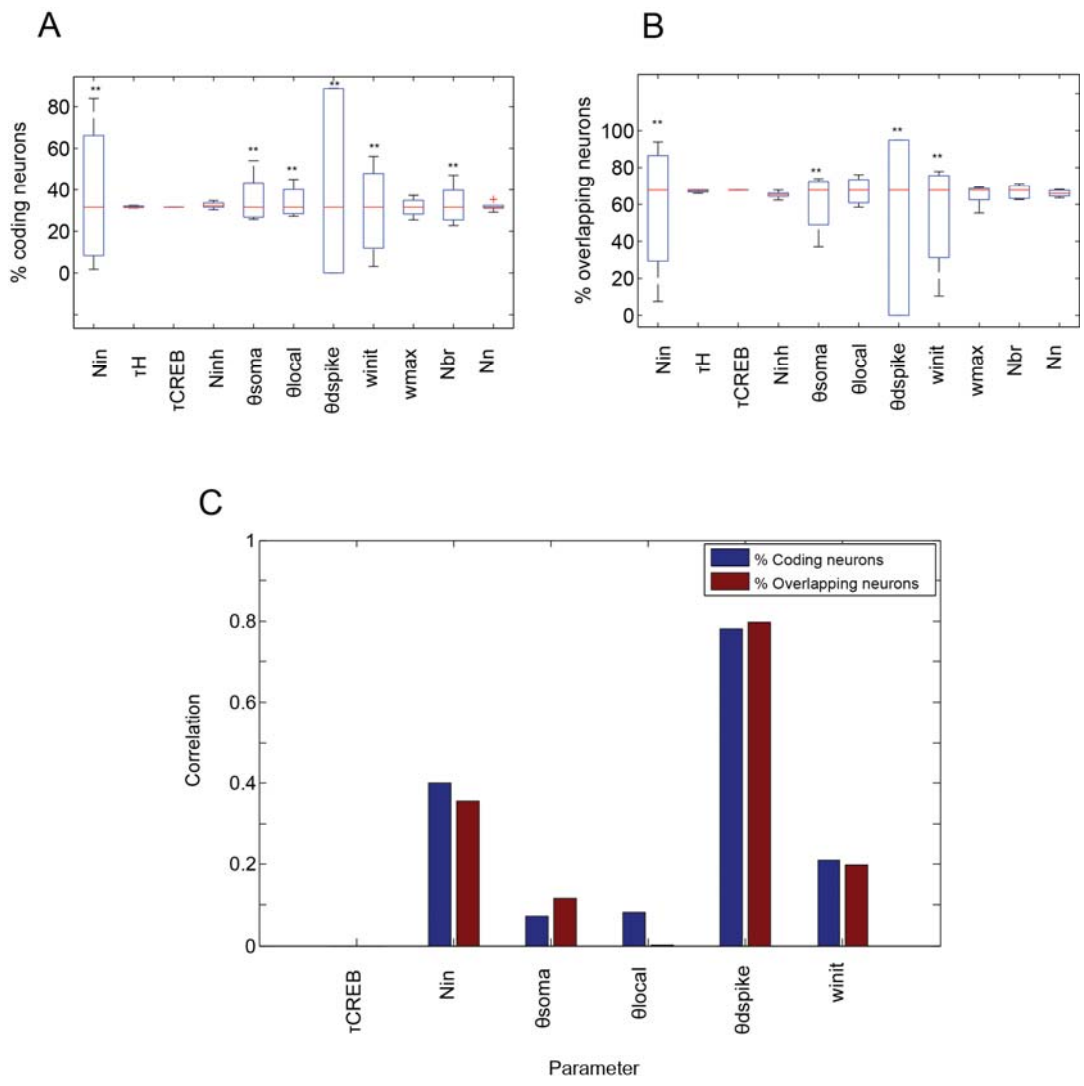

Figure S4; Related to Figure 2B and Figure 4B

Dependence of coding population size and weak-strong memory overlap on model parameters.

A) Box plots indicate the range of values of the coding population for a single memory when each of the model parameters was varied ±30% of its original value listed in Supplemental Tables S1 & S2 (all other listed parameters remained constant). Nin: number of incoming connections, Ninh: number of reciprocal connections between excitatory and inhibitory neurons. Nbr: number of branches per neuron. Nn: number of neurons (See Supplemental Experimental Procedures).
B) Box plots indicate the range of values of the percentage of overlapping coding population between weak and strong memory when each of the model parameters was varied by ±30% of its original value.
C) Pairwise linear (Pearson) correlation coefficients between six of the model parameters, the percentage of coding neurons for single memory encoding (Blue) and the percentage of population overlap during strong-weak memory pairing (Red). In this case all parameters were varied simultaneously between 70%, 100% and 130% of their values listed in Tables S1&S2.

Each box represents 10 simulation trials. Simulations were carried out under the combined S&L condition and Enhanced excitability. The dependence on each model parameter is shown in supplemental figures S2 & S3. **$p<0.01$ one-way ANOVA.

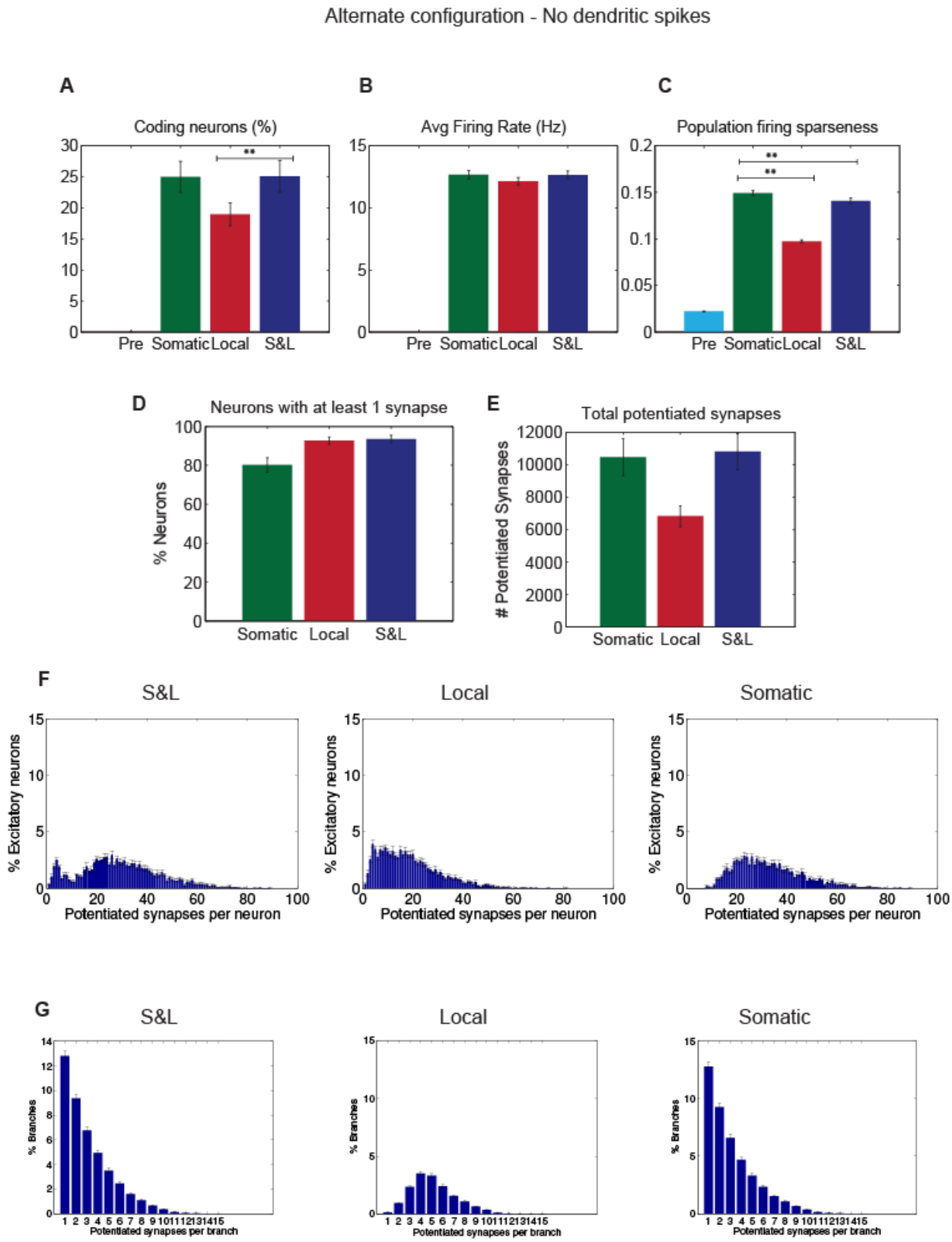

Figure S5; Related to Figure 2.

Properties of synaptic memory allocation without dendritic spikes.

A-E) Properties of coding population under different PRP synthesis conditions and enhanced excitability, but without dendritic spikes. Conventions as in Figures 2 & 3. In these simulations, the number of afferent synapses has been increased by 236% to compensate for the absence of dendritic spikes.

F) Distribution of the number of potentiated synapses per neuron with enhanced excitability. Neurons that did not receive any potentiated synapses are not included. Left: combined Somatic and Local PRP synthesis, middle: Local PRP synthesis, right: Somatic PRP synthesis

G) Distribution of the number of potentiated synapses per dendritic branch. Branches without any potentiated synapses are not included. Left: combined Somatic and Local PRP synthesis, middle: Local PRP synthesis, right: Somatic PRP synthesis

Supplemental Tables

Table S1. Related to Experimental Procedures

Neuronal and plasticity parameters.

Parameter	Description	Model value	Relevant studies
τ_b	Passive dendritic integration time constant	20msec	(Faber et al. 2001)
E_{syn}	Maximum unitary EPSP	4.0 mV	(Larkum & Nevian 2008)
θ_{dspike}	Depolarization threshold for dendritic spiking	30mV	(Losonczy & Magee 2006)
V_{dspike}	Dendritic spike max depolarization	50.0 mV	(Nevian et al. 2007)
E_L	Somatic leakage reversal potential	0 mV	
θ_{soma}	Voltage threshold for somatic spikes	20mV	(Faber et al. 2001)
g_{syn}	Dendritic coupling constant	20 pS	
C	Membrane capacitance	200 pF	
g_L	Leak conductance	6.67 nS	
τ_{AHP}	Adaptation time constant of excitatory neurons	180msec (slow adapting) or 110 msec (fast adapting after learning)	(Faber et al. 2001)
$\tau_{AHP,I}$	Adaptation time constant of interneurons	70 msec	
a_{AHP}	Adaptation conductance increase after a spike	0.18nS	
E_K	Adaptation reversal potential	-10 mV	
τ_{bAP}	Back propagating action potential time constant	15msec	
E_{bAP}	Back propagating action potential max amplitude	30 mV	
a_{Ca}	Calcium influx rate	0.1msec^{-1}	

synTag (x)	Sign of synaptic tag as a function of $[Ca^{2+}]$ (Calcium control model)	$\left(\frac{1.3}{1+exp(-10(10x-3.5.))}\right) - \left(\frac{0.3}{1+exp(-19(10x-2.0))}\right)$	
P_{dend}	Calcium threshold for PRP production in the case of dendritic protein synthesis	2.0 (arbitrary units)	
P_{soma}	Calcium threshold for PRP production in the case of Somatic protein synthesis	18.0 (arbitrary units)	
a_s	Rate of synaptic tag consolidation	6.7 minutes	
τ_H	Time constant of homeostatic synaptic scaling	7 days	
w_{init}	Initial synapse weight	0.2	
τ_{CREB}	Time constant of increased excitability (presumed due to CREB activation)	1.26 hours	

Table S2: Related to Experimental Procedures.

Network size and connectivity

N_n	Number of neurons	500
N_{pyr}	Number of excitatory neurons	400
N_{inh}	Number of inhibitory neurons	100
$N_{branches}$	Number of branches per excitatory neuron	20
$N_{background}$	Background-stimulation input neurons	10
N_{event}	Number of stimulus-carrying input neurons per memory	6 (3 S1 inputs / 3 S2 inputs)
$N_{pyr \rightarrow inh}$	Total number of connections from pyramidal neurons to inhibitory neurons	3200
$N_{inh \rightarrow pyr}$	Total number of connections from inhibitory neurons to pyramidal neurons	4800
$N_{stim \rightarrow pyr}$	Total number of plastic synaptic connections from each set of 6 memory encoding neurons to excitatory neuron dendritic subunits	12800
$N_{background \rightarrow pyr}$	Total number of synaptic connections from background input neurons to excitatory neuron dendritic subunits	1600

Supplemental Experimental Procedures

A network of 500 model neurons was implemented, consisting of excitatory integrate-and-fire neurons with dendritic subunits (80%; 400 neurons) and inhibitory point neurons (20%, 100 neurons). To account for nonlinear dendritic integration reported in pyramidal neurons (Poirazi et al. 2003a; Poirazi et al. 2003b; Polsky et al. 2004; Losonczy & Magee 2006) , each excitatory neuron was modeled as a two-layer structure. This was based on prior work, showing that a two-layer artificial neural network model can reproduce the firing rate of a detailed biophysical CA1 pyramidal neuron model under a wide range of stimulus intensities and distributions (Poirazi et al. 2003b; Jadi et al. 2014). Support for such two stage integration in single pyramidal neurons has also been provided by anatomical studies (Katz et al. 2009). In our model, excitatory neurons have 20 dendritic subunits where synaptic integration and synaptic tagging and capture take place independently. Inhibitory neurons are modeled similarly to excitatory neurons, but with 1 dendritic subunit, that does not generate dendritic spikes. The dendritic subunits contribute to the depolarization of the soma, which acts as the second layer of synaptic integration. Details about the exact values of the parameters listed in the following equations are provided in Table S1.

Dendritic integration

Dendritic subunits integrate incoming synaptic signals independently of each other. Dendritic EPSPs from synaptic inputs are first scaled according to their synaptic weight (see below) and then summed linearly to calculate the dendritic branch voltage, V_b, which decays exponentially with time constant τ_b, as described by the following equation:

$$\tau_b \frac{dV_b}{dt} = \sum_{i,j} w_j E_{syn}\, \delta\left(t - t_{i,j}\right) - V_b \qquad (1)$$

Where $t_{i,j}$ are the times of incoming spikes for synapse j, w_j is the weight of the synapse and E_{syn} is the unitary EPSP. The back propagating action potential V_{bAP} (see below) is summed with V_b to determine the depolarization of the dendrite. When the sum of V_b+V_{bAP} exceeds the dendritic spike generation threshold, θ_{dspike}, a dendritic spike is generated, which causes the voltage of the subunit, V_b to rise instantaneously to V_{dspike}.

Somatic integration

The V_d of each dendritic subunit is scaled by the branch coupling strength B of the dendrite to calculate its contribution to the synaptic input current that it provides to the soma. The sum of all dendritic currents is added to the total inhibitory current received by the neuron and this provides the total input current to the soma, which is modeled as an integrate-and-fire point unit with adaptation (Jolivet et al. 2006). The total current input to the somatic nonlinearity is given by the equation:

$$I_{syn}(t) = g_{syn} \sum_n (B\ V_{b,n}(t)) - IPSC(t) \qquad (2)$$

where *IPSC (t)* is the total inhibitory input that the neuron receives, g_{syn} is the initial dendritic coupling constant, and B is a constant. The above equation ensures that inhibition modulates the somatic output directly, in accordance with experimental data (Markram et al. 2004). The voltage response of the somatic subunit and its spiking output is modeled by an adaptive integrate-and-fire unit. The somatic membrane potential V is given by equations (3) and (4):

$$C\frac{dV}{dt} = -g_L(V - E_L) - g_{AHP}(V - E_K) + I_{syn}(t) \qquad (3)$$

$$\tau_{AHP}\frac{dg_{AHP}}{dt} = a_{AHP}\delta(t - t_{spike}) - g_{AHP} \qquad (4)$$

Where C is the somatic membrane capacitance, g_L is the leak conductance, E_L the resting potential, g_{AHP} is the conductance of the afterhyperpolarization (AHP) current and E_K is the AHP reversal potential. Equation (4) describes adaptive conductance g_{AHP}, where τ_{AHP} is the adaptation time constant, a_{AHP}, the quantal increase of g_{AHP} after a somatic spike which occurs at time t_{spike} and $\delta(t)$ is the Dirac delta. The time constant τ_{AHP} can have two values which correspond to the high and

low excitability levels of the neuron. Increased neuronal excitability has been have been observed after learning and overexpression of CREB (Disterhoft & Oh 2006; Zhou et al. 2009). Accordingly, in our model, if a neuron exceeds the Calcium threshold for somatic PRP synthesis (detailed below), it is considered to take part in the memory engram and its excitability is subsequently increased for 12 hours following learning.

Somatic spiking and reset occurs when the somatic voltage reaches a threshold V_T. The backpropagating action potential is modeled by a depolarization component V_{bAP} which is added to all the dendritic subunits. $V_{bAP}(t)$ is modeled by an exponential:

$$V_{bAP}(t) = E_{bAP}\, e^{-\frac{t}{\tau_{bAP}}} \qquad (5)$$

Where E_{bAP} is the peak of the backpropagating depolarization and τ_{bAP} is the time constant of the *bAP*. The time constant V_{bAP} is large and thus it has a slow tail, which has previously been shown to be required by the calcium control model of plasticity for STDP (Shouval et al. 2002).

Calcium modeling

Calcium acts as the main trigger for the induction of synaptic tags and for the synthesis of PRPs. The total calcium influx during a learning event to a synapse determines the level of calcium C_{syn} which models the calcium concentration near each synapse. Each incoming synaptic spike causes a step increase of calcium, which depends nonlinearly on the local depolarization of the dendritic branch where the synapse resides. We assume that calcium influx upon arrival of a presynaptic spike ΔC_{syn} is primarily through NMDA receptors (Higley & Sabatini 2012) and is thus dependent on the depolarization of the dendritic membrane sigmoidally:

$$\Delta C_{syn} = a_{Ca}\ \frac{1}{1+exp\left(-\frac{V\ \ -30\ mV}{5\ mV}\right)} \qquad (6)$$

where α_{Ca} is the maximum Ca^{+2} influx and $V=V_b+V_{bAP}$

Synaptic Tag generation

The strength and the sign (LTP or LTD) of the synaptic tag are determined according to the Calcium Control Model (Shouval et al. 2002), thus low to intermediate levels of Ca^{2+} cause LTD, while higher levels cause LTP (see Figure 1C). After a learning event, the calcium level C_{syn} determines the sign and magnitude of the synaptic tag according to the function *synTag*. The synaptic tag does not alter the weight of the synapse immediately, but only after the capture of PRPs which are required for consolidation. Synaptic tags in our model decay exponentially with time constant of 1 hour (Figure 1D-E).

Plasticity related proteins production

Plasticity studies have identified a crucial role of somatic protein transcription/translation for the consolidation of synaptic plasticity (Frey et al. 1989; Nguyen et al. 1994). Recent studies, however, suggest that under certain conditions, somatic protein translation may not be needed, and instead dendritic protein translation may be crucial (Kang & Schuman 1996; Huber et al. 2000). Dendrites contain protein synthesis machinery as well as an array of mRNAs coding for plasticity-related proteins (Sutton & Schuman 2006; Cajigas et al. 2012). Studies of synaptic tagging and capture have shown that it is possible for the phenomenon to occur at both the somatic and the dendritic level (Frey & Morris 1997; Govindarajan et al. 2011).

We simulate three conditions of protein production in our model: in the first condition, PRPs are presumed to be produced in the soma of the neuron and made available to all dendritic subunits simultaneously. In the second condition, PRP production is restricted in dendritic subunits and is independent of the PRP synthesis in other dendritic subunits. We refer to the first condition as "somatic PRP synthesis" and the second as "local PRP synthesis". For the two conditions, we define separate calcium thresholds for PRP synthesis. The third condition is the combination of the two, such that at every time point the PRPs available to a synapse is the sum of the globally available PRPs and the locally (branch) available PRPs.

PRP synthesis initiation is modeled as an all-or-none phenomenon. In the case of dendritic PRP synthesis, when the total dendritic calcium level exceeds the dendritic PRP production threshold, $P_{dend,}$, i.e. when $\sum_j C_{syn,j} > P_{dend}$, a PRP transient increase is generated. Accordingly, in the case of Somatic PRP synthesis, a PRP transient is generated when the total

calcium level (sum of all dendritic calcium levels) exceeds the somatic PRP production threshold, P_{soma}, i.e. $\sum_n \left(\sum_j C^n_{syn,j}\right) > P_{soma}$. The time course of a PRP transientis modeled as alpha functions with different time courses:

$$PRP_{soma}(t) = H(t - 20min)\left(\frac{t-20min}{30\ min}\right) exp\left(1 - \frac{t-20min}{-30\ min}\right) \quad (7)$$

$$PRP_{dend}(t) = \left(\frac{t}{15\ min}\right) exp\left(1 - \frac{t}{15\ min}\right)$$

where $PRP_{soma}\ (t)$ is the stereotypical time course of the protein concentration when somatic protein synthesis is triggered at time t, $PRP_{dend}\ (t)$ the time course of the concentration of PRPs in the dendrite when dendritic protein synthesis is triggered at time t and H (t) is the Heaviside step function (see Figure 1B).

When multiple PRP transients have been generated at different time points $t_{PRP,i}$, the total PRP level at any time point is the saturating sum of PRP transients:

$$PRP_{total}(t) = \sum_i \left(1.0 - PRP_{total}(t)\right) PRP\ (t - t_{PRP,i}) \quad (8)$$

Synaptic tag consolidation

Synaptic tags are converted to consolidated synapse weights over time with a rate that is proportional to the value of the tag and the level of PRPs.

$$\Delta w = a_s * synaptictag * PRP_{total}(t) \quad (9)$$

where *synaptictag* is the value of the synaptic tag (positive for LTP, negative for LTD) and a_s is the rate of synaptic tag consolidation. Consolidated synaptic weights are hard-limited in the range [0,1.0].

Dynamic neuronal excitability

Learning has been shown to increase the excitability of neurons participating in the formation of a given memory (Disterhoft & Oh 2006; Silva et al. 2009; Zhou et al. 2009; Frick et al. 2004; Oh et al. 2003; Sehgal et al. 2014). Neurons with increased excitability on the other hand are more likely to participate in the formation of a new memory engram (Zhou et al. 2009; Huang et al. 2008; Kim et al. 2013). The activation of transcription factor CREB has also been found to modulate the excitability of neurons (Dong et al. 2006; Han et al. 2006) through the reduction of the afterhyperpolarization (AHP) current (Lopez de Armentia et al. 2007; Zhou et al. 2009)Therefore, it has been suggested that learning makes cells more amenable to be recruited in future learning events through the activation of CREB (Silva et al. 1998; Benito & Barco 2010; Kim et al. 2014; Silva et al. 2009; Rogerson et al. 2014). Finally, it has been proposed that CREB may also induce the downstream activation of its own repressors (Zhou et al. 2009; Silva et al. 2009), which would lead to the reduction of excitability after a certain period, thus creating a time window of increased neuronal excitability. We simulate the increased excitability through the transient reduction of the AHP current in the neurons in which somatic PRP synthesis is triggered for approximately 12 hours after the learning event.

Homeostatic plasticity

The effect of homeostasis on synaptic weights is modeled using a synaptic scaling rule (Turrigiano 2008). According to this rule, the total synaptic weight of a model neuron remains constant. The synaptic weights, w_j, of each synapse are normalized according to the following equation:

$$\frac{dw_j}{dt} = \frac{1}{\tau_H}\left(1 - \frac{\sum_j w_j}{w_{init}\, N_{syn}}\right) \quad (12)$$

where w_{init} is the initial synapse weight and N_{syn} the total number of synapses in the model neuron. Homeostatic synaptic scaling has a slow time course determined by τ_H, therefore we introduce a large post-learning period in order to simulate its effect.

Interneuron model

Interneurons are modeled similarly to excitatory neurons, but with only 1 dendritic subunit that does not generate dendritic spikes. In addition, interneurons have a different spike adaptation time constant$\tau_{AHP,I}$. Inhibitory afferent and efferent connections are not plastic. Interneurons thus provide feedback inhibition to the local circuit (Figure 1F).

Calibration of plasticity and connectivity and robustness analysis

Learning studies have shown that memories are stored in distributed populations of neurons (Guzowski et al. 1999). During amygdala-dependent fear learning, for example, a large percentage of the lateral amygdala neurons (50-70%) are activated (i.e. receive the sensory stimulus), however only 25-30% of them undergo plasticity during memory storage (Quirk et al. 1995; Repa et al. 2001; Rumpel et al. 2005; Sehgal et al. 2014). This suggests that although sensory input is widely distributed in the lateral amygdala, only a small subset of neurons undergoes plasticity and becomes part of the memory trace.

Accordingly, we calibrated our initial network connectivity and the thresholds of somatic or dendritic Ca^{2+} level that is required for PRP-production so that, after learning of a single memory, its recall of a single memory activates about 30% of this neuronal population (Figure 1). The resulting calibrated parameter values and plasticity thresholds are listed in Tables S1 & S2.

In order to assess the sensitivity of the model to these parameter choices, we analyzed the robustness of the network with respect to 6 parameters: a) the thresholds for somatic and dendritic PRP synthesis, b) the threshold dendritic spiking, c) the time constant of homeostatic plasticity d) the time constant of increased excitability (CREB activation) e) the amount of inhibition, determined by the number of excitatory-to-inhibitory and inhibitory-to-excitatory connections (see tables S1 and S2 for the parameters used in the paper), f) the initial and maximu values of synaptic weights g) the number of branches per neuron, and h) the total number of neurons simulated. We performed a parameter space exploration of these parameters by varying their values from 70% of the value stated in Tables S1&S2 value to 130%.

Analysis of memory engrams

Successful learning of a given memory is assessed by measuring the spiking properties of the excitatory neuronal population during recall. Due to the diffuse connectivity of the network model, a significant percentage of the excitatory population is active during the recall of each memory. We consider neurons to be coding for a specific memory when their average firing frequency during recall is above 10Hz.

In order to assess the sparseness of the population response before and after learning we used the population sparseness measure proposed by Treves & Rolls (Treves & Rolls 1991) subtracted from unity so that higher values correspond to more sparseness:

$$S_T = 1 - \frac{(\sum_j \frac{r_j}{N})^2}{(\sum_j \frac{r_j^2}{N})}$$

Where r_j is the average firing rate of neuron j during memory recall, $j=1...N$, and is N the total number of excitatory neurons. The measure is applied on the distribution of firing rates of all pyramidal neurons in the network before and after training. A narrow distribution with a sharp peak represents a sparser encoding than a less sharp, wider distribution.

In addition to the firing properties of the model network, the structure of memory engrams at the subcellular level is assessed by analyzing the distribution of potentiated synapses after memory encoding. The overlap in the population recruited by different memories is assessed by calculating the ratio of the number of neurons that are activated by both memories over the sum of neurons activated by the two memories. The clustering between different memories in the same branch is assessed by counting the number of branches that contain 2 or more potentiated synapses from both memories over the number of branches that contain at least 2 potentiated synapses from either memories.

Table S1 and Table S2 list the values of all model parameters, and the connectivity properties of the model network. Time was discretized at 1msec during memory encoding events, and at 60 sec during the simulation of ISIs. The simulation code was written in C++ and is available upon request from the authors. Simulations were performed in the CBL-IMBB Linux computing cluster.

Dependence of results on model parameters

In order to ascertain whether the findings presented in the previous sections are sensitive to parameter choices listed in Supplemental Tables S1 & S2, we varied the value of the most important model parameters by up to ±30% of their initial value, one at a time. We measured the effect of each parameter change in two quantities: the coding population size for storing a single memory (Figure 2A) and the coding population overlap between strong and weak memory in the case of weak-strong memory pairing (Figure 4A). As shown in Figure S4A the parameters that had significant effect in coding population size were the number of afferent connections, the PRP thresholds for somatic and local protein synthesis the threshold for dendritic spiking, the initial weights of synapses and the number of branches per neuron. The same set of parameters, except for the number of branches had significant effects in the overlapping population between strong and weak memories (Figure S4B). The change in these measures as a function of increasing parameter values are shown in supplemental figures S2 and S3. Finally, by systematically varying the values of six model parameters, we used linear correlation analysis to assess the effect of each parameter on the two output parameters specified above (coding population and overlap of strong-weak memory). As shown in Figure S4C the number of stimulus-carrying connections (N_{in}), the threshold for dendritic spikes (θ_{dspike}), the somatic PRP threshold (θ_{soma}) and initial synapse weight (w_{init}) had significant effect to both the coding population size and population overlap, while the local PRP threshold (θ_{local}) did not have significant correlation with the population overlap. The largest effects are seen by changes in the number of incoming afferents that affect the probability of different memories impinging on common neurons and the threshold for dendritic spikes, highlighting the importance of active dendritic properties in the formation of neuronal overlaps. The effect of w_{init} is large because a minimum initial weight is needed for reaching the threshold for plasticity induction. This parameter is not crucial as changes in the setting of the model can eliminate this dependence on initial weight values. Overall, our findings remain relatively robust to a number of parameters that are different between types of cortical neurons, such as the number of independent subunits per neuron, and their calcium thresholds for PRP synthesis. The same holds for the time course of slowly acting homeostatic and excitability mechanisms. On the other hand, the ability to generate dendritic spikes and the gating of plasticity by inhibition have a more significant influence in our results (Figure S4C). However, as shown in Figures S2, S3 and S5, even in the complete absence of dendritic spikes, single memory encoding and weak-strong memory interactions take place albeit for unrealistic numbers of afferent connections.

Supplemental References

Benito, E. & Barco, A., 2010. CREB's control of intrinsic and synaptic plasticity: implications for CREB-dependent memory models. *Trends in neurosciences*, 33(5), pp.230–40.

Cajigas, J. et al., 2012. The Local Transcriptome in the Synaptic Neuropil Revealed by Deep Sequencing and High-Resolution Imaging. *Neuron*, 74(3), pp.453–466.

Disterhoft, J.F. & Oh, M.M., 2006. Learning, aging and intrinsic neuronal plasticity. *Trends in neurosciences*, 29(10), pp.587–99.

Dong, Y. et al., 2006. CREB modulates excitability of nucleus accumbens neurons. *Nature neuroscience*, 9(4), pp.475–7.

Faber, E.S., Callister, R.J. & Sah, P., 2001. Morphological and electrophysiological properties of principal neurons in the rat lateral amygdala in vitro. *Journal of neurophysiology*, 85(2), pp.714–23.

Frey, U. et al., 1989. Long-term potentiation induced in dendrites separated from rat's CA1 pyramidal somata does not establish a late phase. *Neuroscience Letters*, 97(1), pp.135–139.

Frey, U. & Morris, R.G.M.G., 1997. Synaptic tagging and long-term potentiation. *Nature*, 385(6616), pp.533–6.

Frick, A., Magee, J. & Johnston, D., 2004. LTP is accompanied by an enhanced local excitability of pyramidal neuron dendrites. *Nature neuroscience*, 7(2), pp.126–35.

Govindarajan, A. et al., 2011. The dendritic branch is the preferred integrative unit for protein synthesis-dependent LTP. *Neuron*, 69(1), pp.132–46.

Guzowski, J.F. et al., 1999. Environment-specific expression of the immediate-early gene Arc in hippocampal neuronal ensembles. *Nat Neurosci*, 2(12), pp.1120–1124.

Han, M.-H. et al., 2006. Role of cAMP response element-binding protein in the rat locus ceruleus: regulation of neuronal activity and opiate withdrawal behaviors. *The Journal of neuroscience*, 26(17), pp.4624–4629.

Higley, M.J. & Sabatini, B.L., 2012. Calcium Signaling in Dendritic Spines. *Cold Spring Harbor perspectives in biology*.

Huang, Y.H. et al., 2008. CREB modulates the functional output of nucleus accumbens neurons: a critical role of N-methyl-D-aspartate glutamate receptor (NMDAR) receptors. *The Journal of biological chemistry*, 283(5), pp.2751–60.

Huber, K.M., Kayser, M.S. & Bear, M.F., 2000. Role for rapid dendritic protein synthesis in hippocampal mGluR-dependent long-term depression. *Science Signaling*, 288(5469), p.1254.

Jadi, M.P. et al., 2014. An Augmented Two-Layer Model Captures Nonlinear Analog Spatial Integration Effects in Pyramidal Neuron Dendrites.

Jolivet, R. et al., 2006. Integrate-and-Fire models with adaptation are good enough: predicting spike times under random current injection. *Advances in neural information processing systems*, 18, pp.595–602.

Kang, H. & Schuman, E.M., 1996. A requirement for local protein synthesis in neurotrophin-induced hippocampal synaptic plasticity. *Science*, 273(5280), pp.1402–1406.

Katz, Y. et al., 2009. Synapse distribution suggests a two-stage model of dendritic integration in CA1 pyramidal neurons. *Neuron*, 63(2), pp.171–7.

Kim, J. et al., 2013. CREB and neuronal selection for memory trace. *Frontiers in neural circuits*, 7(March), p.44.

Kim, J. et al., 2014. Memory recall and modifications by activating neurons with elevated CREB. *Nature neuroscience*, 17(1), pp.65–72.

Larkum, M.E. & Nevian, T., 2008. Synaptic clustering by dendritic signalling mechanisms. *Current opinion in neurobiology*, 18(3), pp.321–31.

Lopez de Armentia, M. et al., 2007. cAMP response element-binding protein-mediated gene expression increases the intrinsic excitability of CA1 pyramidal neurons. *The Journal of neuroscience : the official journal of the Society for Neuroscience*, 27(50), pp.13909–18.

Losonczy, A. & Magee, J.C., 2006. Integrative properties of radial oblique dendrites in hippocampal CA1 pyramidal neurons. *Neuron*, 50(2), pp.291–307.

Markram, H. et al., 2004. Interneurons of the neocortical inhibitory system. *Nature Reviews Neuroscience*, 5(10), pp.793–807.

Nevian, T. et al., 2007. Properties of basal dendrites of layer 5 pyramidal neurons: a direct patch-clamp recording study. *Nature neuroscience*, 10(2), pp.206–14.

Nguyen, P. V, Abel, T. & Kandel, E.R., 1994. Requirement of a critical period of transcription for induction of a late phase of LTP. *Science*, 265(5175), pp.1104–1107.

Oh, M.M. et al., 2003. Watermaze learning enhances excitability of CA1 pyramidal neurons. *Journal of Neurophysiology*, 90(4), pp.2171–2179.

Poirazi, P., Brannon, T. & Mel, B.W., 2003a. Arithmetic of subthreshold synaptic summation in a model CA1 pyramidal cell. *Neuron*, 37(6), pp.977–87.

Poirazi, P., Brannon, T. & Mel, B.W., 2003b. Pyramidal neuron as two-layer neural network. *Neuron*, 37(6), pp.989–99.

Polsky, A., Mel, B.W. & Schiller, J., 2004. Computational subunits in thin dendrites of pyramidal cells. *Nature neuroscience*, 7(6), pp.621–7.

Quirk, G.J., Repa, C. & LeDoux, J.E., 1995. Fear conditioning enhances short-latency auditory responses of lateral amygdala neurons: parallel recordings in the freely behaving rat. *Neuron*, 15(5), pp.1029–39.

Repa, J.C. et al., 2001. Two different lateral amygdala cell populations contribute to the initiation and storage of memory. *Nature Neuroscience*, 4(7), pp.724–731.

Rogerson, T. et al., 2014. Synaptic tagging during memory allocation. *Nature Reviews Neuroscience*, 15, pp.157–169.

Rumpel, S. et al., 2005. Postsynaptic receptor trafficking underlying a form of associative learning. *Science (New York, N.Y.)*, 308(5718), pp.83–8.

Sehgal, M., Ehlers, V.L. & Moyer, J.R., 2014. Learning enhances intrinsic excitability in a subset of lateral amygdala neurons. *Learning & Memory*, 21(3), pp.161–170.

Shouval, H.Z., Bear, M.F. & Cooper, L.N., 2002. A unified model of NMDA receptor-dependent bidirectional synaptic plasticity. *Proceedings of the National Academy of Sciences*, 99(16), pp.10831–10836.

Silva, a J. et al., 1998. CREB and memory. *Annual review of neuroscience*, 21, pp.127–48.

Silva, A.J. et al., 2009. Molecular and cellular approaches to memory allocation in neural circuits. *Science (New York, N.Y.)*, 326(5951), pp.391–5.

Sutton, M.A. & Schuman, E.M., 2006. Dendritic protein synthesis, synaptic plasticity, and memory. *Cell*, 127(1), pp.49–58.

Treves, A. & Rolls, E., 1991. What determines the capacity of autoassociative memories in the brain? *Network: Computation in Neural Systems*, 2(4), pp.371–397.

Turrigiano, G.G., 2008. The self-tuning neuron: synaptic scaling of excitatory synapses. *Cell*, 135(3), pp.422–35.

Zhou, Y. et al., 2009. CREB regulates excitability and the allocation of memory to subsets of neurons in the amygdala. *Nature neuroscience*, 12(11), pp.1438–43.